Particle Size Distribution Control in Emulsion Polymerization

Ashwini Sood

Department of Chemical Engineering, Harcourt Butler Technological Institute, Kanpur 208 002, India

Received 2 December 2002; accepted 19 March 2003

ABSTRACT: Effects of the operating policies—the initial initiator amount; the initial emulsifier amount; the monomer addition mode: batch or semibatch; and the monomer addition rate under "monomer-starved conditions" for the control of particle size distribution (PSD)—were studied through a model that simulates batch and semibatch reactor operations in conventional emulsion polymerization. The population balance model incorporates both the nucleation stage and the growth stage. The full PSDs were reported, which have normally been omitted in earlier studies. It was shown through simulations that the broadness of the distributions, both initial (obtained after the end of nucleation) and final (after complete conversion of monomer), can be controlled by the initial initiator amount and the emulsifier amount. The higher initiator amounts and the lower emulsifier amounts favor narrower initial and final distributions. The shape of the initial PSDs and the trends in the average size and range were preserved with subsequent addition of monomer in the batch or in the semibatch mode, although the final PSD was always considerably narrower than that of the initial PSD. The addition of monomer in the semibatch mode gave narrower distribution compared to that of the batch mode, and also, lower monomer addition rates gave narrower distributions (larger average sizes), which was a new result. It was further shown through simulations that, under monomer-starved conditions, the reaction rate closely matched the monomer feed rate. These conclusions are explained (1) qualitatively—the shorter the length of the nucleation stage and the larger the length of the growth stage (provided the number of particles remains the same), the narrower is the distribution; and (2) mathematically—in terms of the "self-sharpening" effect. Experimental evidence in favor of the self-sharpening effect was given by analyzing the experimental particle size distributions in detail. The practical significance of this work was proposed. © 2004 Wiley Periodicals, Inc. J Appl Polym Sci 92: 2884–2902, 2004

Key words: emulsion polymerization; particle nucleation; growth; modeling; particle size distribution

INTRODUCTION

Particle size distribution (PSD) is a key parameter in the emulsion polymerization process; it directly influences the end-use properties of the final latex such as viscosity.[1] Nucleation, growth, and coalescence of the latex particles govern the evolution of the latex particle size distribution in emulsion polymerization, in general.[2] The role of coalescence (in providing stability to monomer droplets in miniemulsion polymerization) was studied separately[3] and it was concluded that under normal reactor conditions in emulsion polymerization, particles remain stable and coalescence can be neglected. Most industrial reactors for emulsion polymerization of conventional monomers, like styrene, operate at a high level of emulsifiers and thus the particles are stable and do not undergo coalescence, and also, at high emulsifier levels, the dominant nucleation mechanism is the micellar nucleation. A model that incorporated nucleation in micelles and growth was developed and used to study the effect of certain operating policies that would give narrow or monodisperse seed distributions.[4] Open-loop control policies that can influence the course of development of PSD in emulsion polymerization are highly desirable to produce emulsion polymers with desired PSD. In this article, the roles of initial initiator amount, initial emulsifier amount, monomer addition mode (batch or semibatch), and monomer addition rate under "monomer-starved" conditions in controlling the PSD are studied through a model that simulates batch and semibatch reactor operations in conventional emulsion polymerization.

Correspondence to: ashwinisood@rediffmail.com.

Journal of Applied Polymer Science, Vol. 92, 2884–2902 (2004)
© 2004 Wiley Periodicals, Inc.

MODEL DEVELOPMENT

Emulsion polymerization follows the kinetics of free-radical–initiated vinyl addition polymerization superimposed on the heterogeneous colloidal latex system. A typical emulsion polymerization reactor therefore consists of many components and phases, simultaneously undergoing numerous chemical reactions and mass-transfer processes and with strong interactions. The important physical and chemical events in emulsion polymerization include radical generation, particle nucleation, chain propagation, chain termination,

mass transfer of radicals, monomer(s) and emulsifier(s) to and from the latex particles, particle coalescence, variation of termination rate constant, and the propagation rate constant with conversion. A general modeling framework, incorporating all the relevant mechanisms, can be very complex[5] and thus only few models for full PSD are reported in the open literature.[5,8,14,17–19] Such a framework consists of a population balance equation that accounts for the change in the number of particles of a given size attributed to growth and coalescence. The nucleation term provides the boundary condition for this infinite-order partial-differential/integral equation system and accounts for the change in number of particles at the boundary or the initial micellar size.

These equations are coupled to the phenomena occurring in the various phases: the particles, the droplets, and the aqueous phase. This coupling is represented in terms of the overall reactor balances for reactor volume, aqueous phase, monomer, polymer, initiator, emulsifier and electrolyte, aqueous phase balances for monomer, micelles and radicals, equations describing the monomer concentration inside the particle, and the number of radicals inside the particle. These parameters together provide the particle growth rate and the nucleation rate, which in general includes all the different nucleation mechanisms (e.g., micellar, homogeneous, coagulative); and, in monomer droplets, the coagulation rate. The resulting system of equations to be solved consists of partial-differential/integral equations, coupled ordinary differential equations, nonlinear algebraic equations, and Bessel functions. The solution of such a model poses a challenge to any model developer. The approach that is being followed consists of modeling and solving special cases relevant to a given emulsion polymerization system. In a subset of the detailed model model,[5] the coalescence phenomenon was not included and nucleation (micellar) and particle growth attributed to polymerization were incorporated.[4] This model was used to study the effects of the following operating variables on the PSD: (1) the initial initiator amount, (2) the initial emulsifier amount, and (3) the reactor temperature, on the seed PSD for conventional emulsion polymerization when emulsifier is present above the critical micelle concentration (cmc) in the reactor. Neglecting coalescence, the population balance model reduces from a system of partial-differential/integral equations to a system of partial-differential equations. This system of equations is solved using orthogonal collocation. Details of this method and its extension to orthogonal collocation on finite elements will be reported in a subsequent article.

In a typical industrial emulsion polymerization reactor, an initial emulsion preparatory stage is considered. In this stage, a small amount of monomer was emulsified in the presence of mild agitation (36 or 72 rpm for a 50-L pilot-plant reactor) and stabilizers, and subsequently polymerized by addition of thermal initiators like potassium persulfate and rise in reactor temperature, by passing either steam or hot water or both through the external jacket. The remainder of the monomer was subsequently added at a steady rate over a period of 5–6 h and polymerized simultaneously under more or less isothermal conditions. The initial preparatory stage is called "seeding" or the "seed stage." The second stage of monomer addition is called "feeding." This is followed by the last stage where the unreacted monomer reacts to near completion. A mathematical model, applicable to such a system for the batch and the semibatch reactor operations, for conventional emulsion polymerization, involving all the aforementioned three stages, is given below.

Physical picture

The model simulates an isothermal, well-stirred, semibatch emulsion polymerization reactor. Polymer particles, formed through micellar nucleation or present as seed, act as the site of polymerization. The monomer is partitioned among the aqueous phase particle phase and monomer droplets; its concentration in the particle phase was determined by the thermodynamic balance among these phases. The net flux of radicals to the growing particles, determined by the rate of radical entry into, termination inside, and exit from the particles, determines the average number of radicals in them. Monomer concentration and the average number of radicals within a particle determine its growth rate. The emulsifier stabilizes the growing particle surface. The concentration of the emulsifier in the reactor determines the nucleation of new particles. When present above the cmc and that required to stabilize the existing particle surface, the emulsifier forms micelles, which act as nucleation sites. Differences in the nucleation times and growth rates of the various particles result in differences in their sizes and determine the average size and broadness of the resulting PSD.

Overall reactor balances

The overall reactor balances include the balances for monomer [M], polymer [P], emulsifier [E], and initiator [I] and balances for the volume of reaction mixture (V_R) and volume of the aqueous phase (V_W). The material balances, which express the rate of change of moles of each of the species, contain accumulation and reaction terms (where appropriate). The volume of the reaction mixture changes because of density differences between the monomer and the polymer.

$$\frac{d[M]_R V_R}{dt} = Q_M[M]_f - R_p V_R \quad (1)$$

$$\frac{d[P]_R V_R}{dt} = R_p - V_R \quad (2)$$

where $R_p \equiv$ rate of polymerization, expressed as

$$k_p \frac{\rho_M}{MW_M} \int_{V_M}^{\infty} F(v, t)\Phi i \, dv$$

$$\frac{d[E]_R V_R}{dt} = Q_E[E]_f \quad (3)$$

$$\frac{d[I]V_W}{dt} = Q_I[I]_f - k_d[I]V_W \quad (4)$$

$$\frac{dV_R}{dt} = Q_M + Q_E + Q_I - \left(\frac{1}{\rho_M} - \frac{1}{\rho_p}\right) R_p MW_M V_R \quad (5)$$

$$\frac{dV_W}{dt} = Q_E + Q_I \quad (6)$$

where Q_M, Q_E, and Q_I are the volumetric flow rates of the monomer, emulsifier, and initiator, respectively; R_p is the rate of polymerization; V_R is the volume of the reaction mixture; $F(v, t)$ is the number density of the particles; k_p is the propagation rate constant; k_D is the initiator decomposition constant; ρ_M is the density of the monomer; ρ_p is the density of polymer; 70 is the monomer volume fraction in the particle; i is the average number of radicals in the particle; MW_M is the molecular weight of the monomer; and V_M is the volume of the micelle.

Aqueous phase balances

Aqueous phase balances involve the balance for the radical, micelles, and the dissolved monomer.

Equation (7) combines the rates of radical generation in the aqueous phase, termination in the aqueous phase, entry into particles, entry into micelles, and exit from the particles. A quasi–steady-state assumption is used for radical balance.

$$2k_d[I]V_W - k_{tw}[R]^2 V_W - 4\pi k_{mp}[R]N_a \int_{V_M}^{\infty} F(v, t)V_R r^n \, dv \times 4\pi k_{mm} V_m^n [R]N_a[m]V_W + \int_{V_M}^{\infty} k_{de}(v)F(v, t)V_R i \, dv = 0 \quad (7)$$

where V_W is the volume of the aqueous phase, $[R]$ is the aqueous phase radical concentration, N_a is Avogadro's number, k_{tw} is the termination rate constant in the aqueous phase, k_{mp} is the radical entry rate coefficient in the particle, k_{mm} is the radical entry rate coefficient in the micelle, $[m]$ is the micellar concentration, k_{de} is the radical exit rate coefficient, i is the average number of radicals in the particle, and n is the exponent that describes the radical capture model (either diffusion controlled or collision controlled).

The emulsifier distributes itself among the particle surface, monomer droplets, and the aqueous phase. In conventional emulsion polymerization, where the total surface area of monomer droplets is initially an order of magnitude less than the micelles that decreases further as the polymerization progresses, the amount of emulsifier adsorbed on the monomer droplet can be neglected. The free emulsifier ($[E]_W$), which is the amount of emulsifier in the aqueous phase in excess of that required to stabilize the growing particle surface (A_P) and that dissolved in the aqueous phase (article micellar concentration $[E]_{\text{cmc}}$), forms the micelles. The following equations represent the micellar balance:

$$[m] = 0 \quad \text{if } [E]_W \leq [E]_{\text{cmc}} \quad (8)$$

otherwise,

$$[m] = ([E]_W - [E]_{\text{cmc}}) \frac{MW_E N_a a_{em}}{4\pi r_m^2}$$

where

$$[E]_W V_W = [E]_R V_R - \frac{A_P}{a_{ep} N_a} \quad \text{where}$$

$$A_P = \int_{V_m}^{\infty} F(v, t)V_R V^{2/3} \, dv$$

where MW_E is the molecular weight of the emulsifier, r_m is the radius of the micelle, and V is the volume of the particle.

The amount of monomer dissolved in the aqueous phase ($[M]_W V_W$) is obtained by the difference between the total amount of monomer in the reactor ($[M]_R V_R$) and the monomer present inside the particles and the monomer droplets ($[M]_D V_D$).

$$[M]_W V_W = [M]_R V_R - \frac{\rho_M N_a}{MW_M} \times \int_{V_M}^{\infty} F(v, t) V_R v\Phi \, dv - [M]_D V_D \quad (9)$$

where ϕ is the monomer volume fraction in the particle.

Population balance equation

The population balance equation, expressed in terms of the mass of polymer in the particle m_p as the size variable, without the coalescence term, is given by

$$\frac{\partial[F(m_p, t)V_R]}{\partial t} + \frac{\partial[R_g F(m_p, t)V_R]}{\partial m_p} = 0 \quad (10)$$

Boundary condition

$$\frac{\partial[F(m_p, t)V_R]}{\partial t} = R_n(t)$$

Initial condition

$$F(m_p, t) = 0$$

The above equation uses the mass of polymer in the particle (m_p) as the internal coordinate. Rewriting the population balance with the birth time (t') as the internal coordinates, one obtains

$$\frac{\partial[F(t', t)V_R]}{\partial t} = 0; \quad F(t', t)V_R/t = t' = R(t') \quad (11)$$

Although the birth time and the mass of the polymer in the particle are mathematically equivalent [$F(v, t) = F(m_p, t) = F(t', t)$], the birth time description is computationally more attractive. By formulating the problem in birth time, the divergence term vanishes, and thus eq. (11) has the solution

$$F(t', t)V_R = R_n(t') \quad (12)$$

Evaluation of the rate of particle nucleation (R_n) and evaluation of the particle growth rate (R_g) are discussed below.

Micellar nucleation

The rate of micellar nucleation (R_n) will be given by the rate of radical entry into the micelles. Radical entry into micelles (and latex particles) has been postulated to take place by different mechanisms, the two important ones of which are radical entry resulting from diffusion and radical entry resulting from collision. In this work, the rate of radical entry in micelles (R_{em}) is given as

$$R_{em} = k_{mm} 4\pi (r_m)^n [R] N_a [m] V_W \quad (13)$$

The choice of $n = 1$ gives the diffusion model for entry, whereas for the collision model, $n = 2$. The rate of radical entry is coupled to the aqueous phase radical balance, which is given by eq. (7).

By neglecting the aqueous phase termination, and solving the resulting equation for [R], one obtains

$$[R] = \frac{2fk_d[I]V_W + \int_{V_M}^{\infty} k_{de}(v)F(v, t)V_R i(v) \, dv}{4\pi k_{mm}(r_m)^n [m] N_a V_W + 4\pi k_{mp} \int_{V_M}^{\infty} F(v, t)V_R r^n \, dv} \quad (14)$$

By substituting [R] from eq. (14) into eq. (13), one obtains the expression used in the present simulation studies for the rate of micelle nucleation:

$$R_n = 4\pi k_{mm}(\gamma_m)^n [m] N_a V_W \times \frac{2fk_d[I]V_W + \int_{V_M}^{\infty} k_{de}(v)F(v, t)V_R i(v) \, dv}{4\pi k_{mm}(r_m)^n [m] N_a V_W + 4\pi k_{mp} \int_{V_M}^{\infty} F(v, t)V_R \gamma^n \, dv} \quad (15)$$

Particle growth

The particle growth rate (R_g) is given by eq. (16), which defines the rate of reaction [in g (polymer)/s) in a particle having i number of radicals and monomer volume fraction Φ:

$$R_g \equiv \frac{dm_p}{dt} = \frac{k_p i \Phi \, dm}{N_a} \quad (16)$$

The volume of the monomer swollen latex particle (v) can be related to the mass of polymer (m_p) in it by

$$v = \frac{m_p}{d_p(1 - \phi)}$$

The two equations, which together give the volume of the latex particle at any time, contain two variables: the monomer volume fraction in the particle (Φ) and the number of radicals inside the particle (i). The evaluation of these variables is discussed in the following sections.

Monomer volume fraction in the particle

Monomer diffusion into the polymer particles ordinarily occurs at a fast rate.[6,7] Thus, one can make the

quasi–steady-state assumption that the concentration of monomer inside the particles is at its equilibrium value at all times. The equilibrium concentration of monomer can be obtained from eq. (17), given by Min and Ray,[8] which is an extension of that developed by Morton et al.[9]:

$$\frac{2\gamma MW_M}{r\rho_M R_G T} + [1 - \Phi + \ln \Phi - \chi(1 - \Phi)^2] = \ln\left(\frac{[M]_W}{[M]_{sat}}\right) \quad (17)$$

where γ is the interfacial tension, r is the particle radius, R_G is the universal gas constant, T is the absolute temperature, χ is the Flory–Huggins interaction parameter, $[M]_W$ is the monomer concentration in the aqueous phase, and $[M]_{sat}$ is the aqueous phase monomer concentration at saturation.

The above equation results from the balance between the gain in free energy caused by the increase in the interfacial area on swelling, the loss in free energy caused by the mixing of the monomer with the polymer, and the gain in free energy caused by the separation of monomer from the aqueous phase. This equation is coupled to the monomer balance because of the presence of monomer in the aqueous phase. The aqueous phase monomer concentration ($[M]_W$) can be determined by using eq. (9).

When monomer droplets are present in the reactor, the aqueous phase is saturated ($[M]_W = [M]_{sat}$). Then Φ can be calculated from eq. (17); however, when the monomer droplets are absent ($[M]_D = 0$), eqs. (9) and (17) must be solved simultaneously for Φ and $[M]_W$. An important simplification can be made by neglecting the first term in eq. (17), which accounts for the gain in the free energy caused by an increase in the interfacial area on swelling. This simplification enables one to compute Φ independently of particle size. This results in a significant computational advantage because now the two equations need not be solved for different values of particle radius, at each integration step. By combining eqs. (9) and (17), one obtains

$$[M]_{sat}V_W \exp[1 - \Phi + \ln \Phi + \chi(1 - \Phi)^2] - [M]_R V_R - [M]_P V_P = 0 \quad (18)$$

This equation can be solved for Φ, for a given value of V_W; $[M]_R V_R$; and $[M]_P V_P$ (which can be obtained by solving the overall reactor balances for the aqueous phase, monomer and polymer).

Average number of radicals per particle

The average number of radicals per particle is determined by the rate of radical entry into, exit from, and termination inside, the particle. This is given by the quasi–steady-state eq. (19), which is the Smith–Ewart recursion relation[10]:

$$k_e[F_{i-1}(v, t) - F_i(v, t)] + k_{de}[(i + 1)F_{i-1}(v, t) - iF_i(v, t)] + \frac{k_i}{2vN_a}[(i + 2)(i + 1)F_{i-2}(v, t) - i(i - 1)F_i(v, t)] = 0 \quad (19)$$

where k_e is the radical entry rate coefficient and k_t is the radical termination rate constant inside the particle.

The proposed Stockmayer–O'Toole[11,12] relationship for the above equation, with respect to the average number of radicals per particle [($i(v, t)$], is given by

$$i(v, t) = \sum_{i=0}^{\infty} \frac{iF_i}{F(v, t)} = \frac{a}{4}\frac{I_b(a)}{I_{b-1}(a)} \quad (20)$$

where $I_b(a)$ is the modified Bessel function of the first kind of order b and argument a, and

$$a = 4\left(\frac{vN_a k_e}{k_t}\right)^{1/2} \quad \text{and} \quad b = \frac{2vN_a k_{de}}{k_t}$$

where parameter a accounts for the relative importance of radical entry with respect to radical termination, and parameter b accounts for the relative importance of radical exit with respect to radical termination inside the particle.

For this work, the continued fraction form, first used by Ugelstad et al.,[13] is used:

TABLE I
Values of Parameters Used in Simulations

Parameter	Value
r_m	2.5×10^{-7} cm
$a_{em} = a_{ep}$	35×10^{-16} cm^2/molecule
E_{cmc}	0.0005 g/cm^3
f	0.5
k_d	$1.8 \times 10^{17}\exp(-34100/R_gT)$ s^{-1}
k_{de}	0.0
$k_{mm} = k_{mp}$	28
k_p	$1.8 \times 10^{12}\exp(-104000/R_gT)$ cm^3 mol^{-1} s^{-1}
k_t	$6.52 \times 10^{16}\exp(-8870/R_gT)$ cm^3 mol^{-1} s^{-1}
$[M]_{sat}$	2.6×10^{-6} g mol^{-1} cm^3
ϕ_{sat}	0.6
γ	3.41 dyn/cm
ρ_M	0.906 g/cm^3
ρ_p	1.04 g/cm^3
MW_M	104.15 g g^{-1} mol^{-1}
MW_I	270.33 g g^{-1} mol^{-1}
MW_E	288.1 g g^{-1} mol^{-1}
n	2

TABLE II
Conditions for Different Simulations Runs

Simulation	Temperature (°C)	Seed monomer (g)	Water (g)	Emulsifier (g)	Initiator (g)	Monomer added (g)	Mode
1	50	20	500	2.5	1.0	230	Batch
2	50	20	500	2.5	2.0	230	Batch
3	50	20	500	4.0	2.0	230	Batch
4	50	20	500	4.0	2.0	230	2.5 mL/min
5	50	20	500	4.0	2.0	230	1.25 mL/min
6	50	20	500	4.0	2.0	230	2.5 and 5.0 mL/min

$$i = \frac{a}{4}\frac{I_b(a)}{I_{b-1}(a)} = \frac{1}{2}\frac{a^2}{b}\frac{4a^2}{b+1}\frac{4a^2}{b+2}\cdots \qquad (21)$$

MODEL SOLUTION

The mathematical framework consists of the population balance equation, which is a hyperbolic particle differential equation. The model also contains simultaneous ordinary differential equation representing the overall reactor balances, algebraic equations representing the aqueous phase balances and the monomer partitioning among different phases, and Bessel functions representing the average number of radicals inside the particle. Efficient numerical methods are needed to solve the above system of equations.

An efficient method is needed to solve the population balance equation. Especially important is the efficient integration of the total particle distribution to obtain an accurate evaluation of terms like the total particle surface area and the reaction rate without investing large amounts of computer time and storage. The numerical technique that seems the best for solving the population balance equation is orthogonal collocation. This method will be considered in detail and reported in a subsequent article.

Numerical implementation

IMSL MATH/LIBRARY version 1.1 Fortran subroutines were used to numerically solve the modeling equations. Subroutine IVPAG, based on the gear method, was used to solve the initial value ordinary differential equations; subroutine ZREAL, which uses the Muller method, was used to solve the nonlinear algebraic equation to obtain the value of monomer volume fraction inside the particle. As stated earlier, the continued fraction form developed by Ugelstad et al.[13] was used to evaluate the average number of radicals inside the particles.

Effects of initiator and emulsifier charge on PSD

As evident from eq. (15), the initiator concentration and the emulsifier concentration (or micelle concentration) will affect the rate of particle nucleation. In fact, in batch operations of emulsion polymerization reactors, the initial amount of emulsifier and initiator in the recipe is properly formulated to give the desired PSD, which may vary from a monodisperse to a narrow or a broad unimodal distribition. Styrene (monomer), potassium persulfate (initiator; popularly known as PPS), and sodium lauryl sulfate (emulsifier; popularly known as SLS) are considered in this study. The necessary physicochemical and kinetic parameters for this system were taken from the literature[14] and are given in Table I. In this section, three different simulation runs are considered (Table II). These runs vary in the amount of initiator and emulsifier charged in the initial recipe. After the nucleation stage, the remaining monomer was charged in the batch mode. For all the simulation runs, the amount of total monomer charged was 250 g and the amount of water charged was 500 g. Usually, in experimental studies, the total solid content is kept around 30%, and the

TABLE III
Results for Different Simulation Runs

Simulation	Duration of nucleation (min)	Particles formed	Reaction time (min)	Volume average radius (nm)	Range (nm)
1	10.30	0.943×10^{18}	195.25	40.89	2.5
2	6.46	1.10×10^{18}	166.25	38.73	1.7
3	15.47	2.07×10^{18}	87.25	32.14	3.1
4	15.47	2.07×10^{18}	149.0	40.36	2.1
5	15.47	2.07×10^{18}	238.0	40.40	2.1
6	15.47	2.07×10^{18}	137.0	39.56	2.1

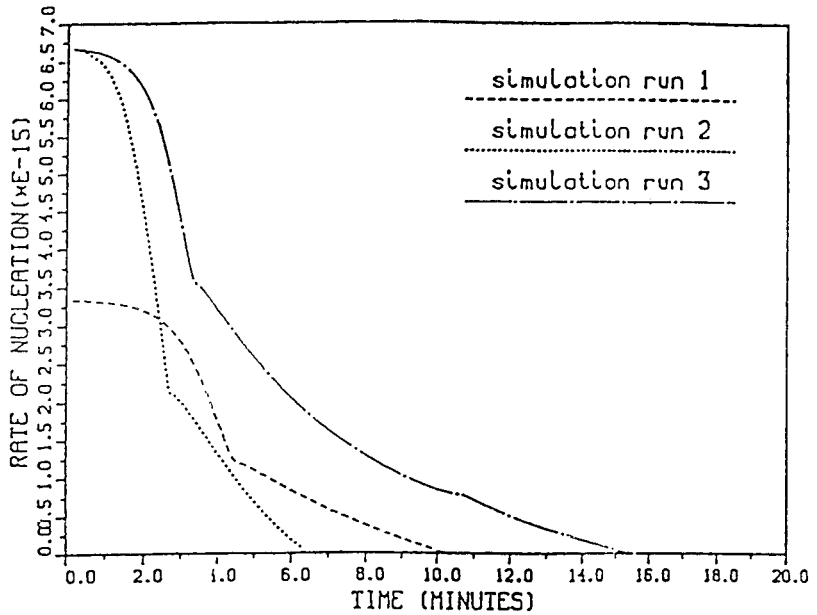

Figure 1 Rate of nucleation for simulations 1, 2, and 3.

monomer in the seed recipe is normally 8–10% of the total recipe weight. The above amounts correspond to these considerations. The effects of emulsifier and initiator amount on the duration of nucleation, the total number of particles formed, the total reaction time, volume average radius, range (Table III), and the full particle size distribution (see Figs. 2 and 3 below) were investigated. In this work, the full particle size distributions are reported, which have not generally received attention in previous works.

As can be seen from Figure 1, for these runs both the rate of nucleation and the duration of nucleation vary. For a given amount of emulsifier (simulations 1 and 2), the duration of nucleation decreases, with the increase in initiator amount. The greater the initiator concentration, the higher will be the rate of radical generation. Because of this, a greater number of particles will initially be initiated (as shown in Fig. 2); as these particles grow, they will consume more emulsifier (from uninitiated micelles) to stabilize their growing

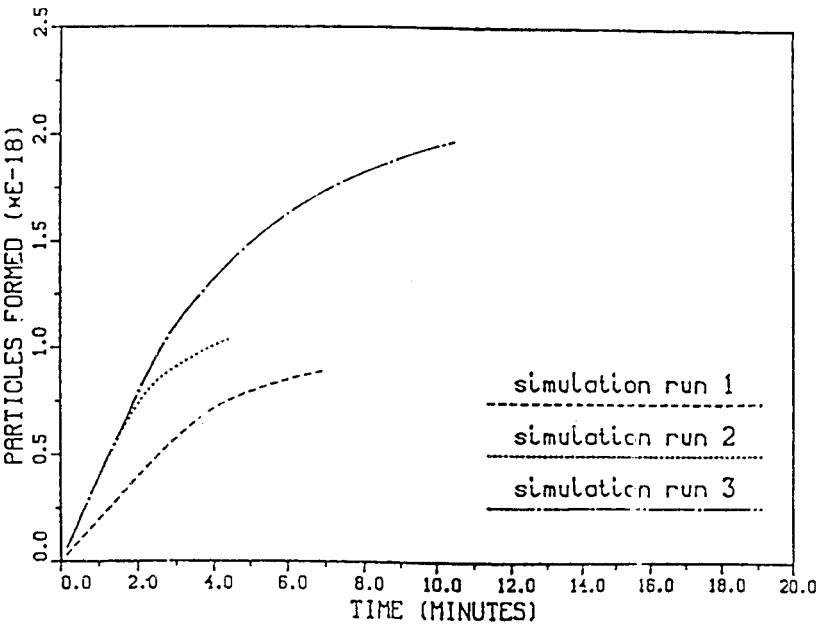

Figure 2 Number of particles formed for simulations 1, 2, and 3.

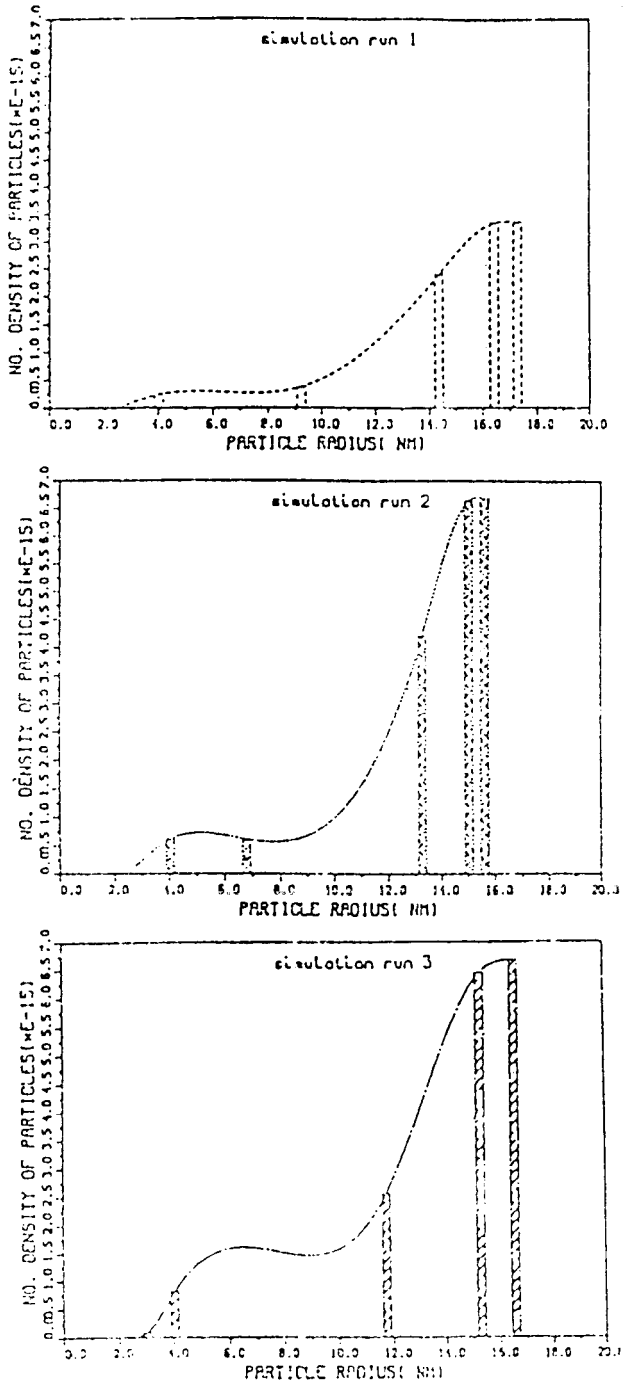

Figure 3 Full particle size distribution (initial) for simulations 1, 2, 3.

surface area. Therefore, for higher concentration, micelles will be depleted at a faster rate, resulting in the decrease in nucleation period. For a given amount of initiator (simulation runs 2 and 3), both the duration of nucleation and the number of particles formed increase significantly, with the increase in emulsifier amount. This is attributed to the fact that the higher the emulsifier level, the greater the number of particles that can be initiated and the longer the time before which the free emulsifier is depleted. The resulting particle size distributions at the end of the nucleation (or seeding) for these runs are given in Figure 3. The vertical bar represents the distribution at the colloca-

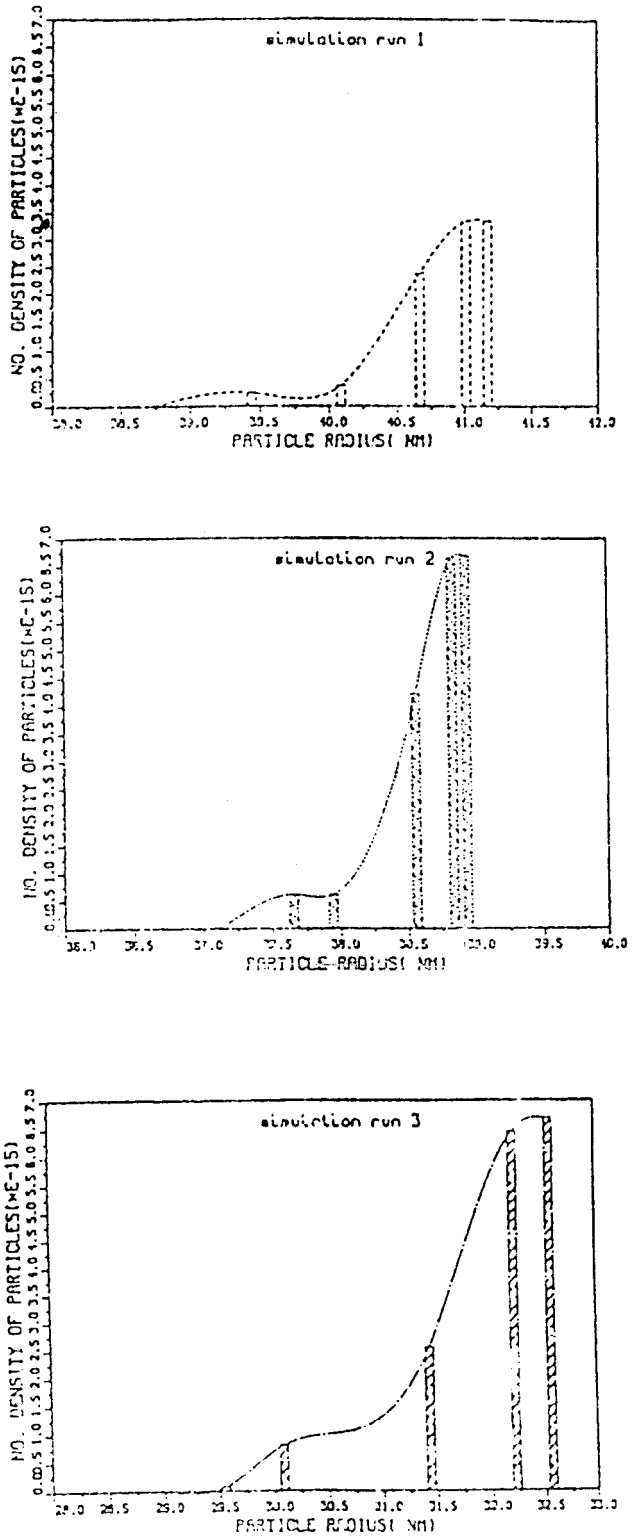

Figure 4 Full particle size distribution (final) for simulations 1, 2, and 3.

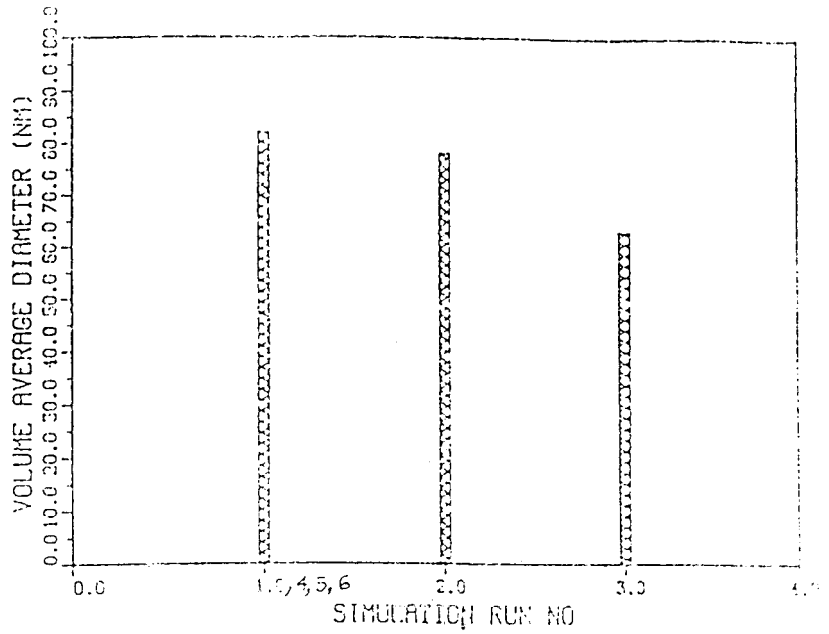

Figure 5 Volume-average diameters for simulations 1, 2, and 3.

tion points (six considered for all simulations) and the continuous curve is obtained by interpolation between these points. As can be seen, the particle radii vary from micellar dimensions to around 17 nm, the range of the particle radii (maximum − minimum) for the three runs being 15, 13, and 14 nm. Range can be considered as a measure of the broadness of the duration. Thus, it can be concluded that with the increase in initiator amount, the breadth (or the range) of the distribution decreases or the distribution becomes narrower. With the increase in the emulsifier amount, the distribution becomes broader. With the subsequent addition of the same amount of monomer (giving 33% total solids), these distributions grow in size.

Figure 4 shows the final PSD at the end of complete run [seed stage + monomer addition stage + monomer reaction stage to completion (<2% unreacted monomer)]. The final particle radii vary between 29.5 and 41.2 nm. The final ranges for the three runs are 1.75, 1.7, and 3.1 nm. Thus, the trends in the range are

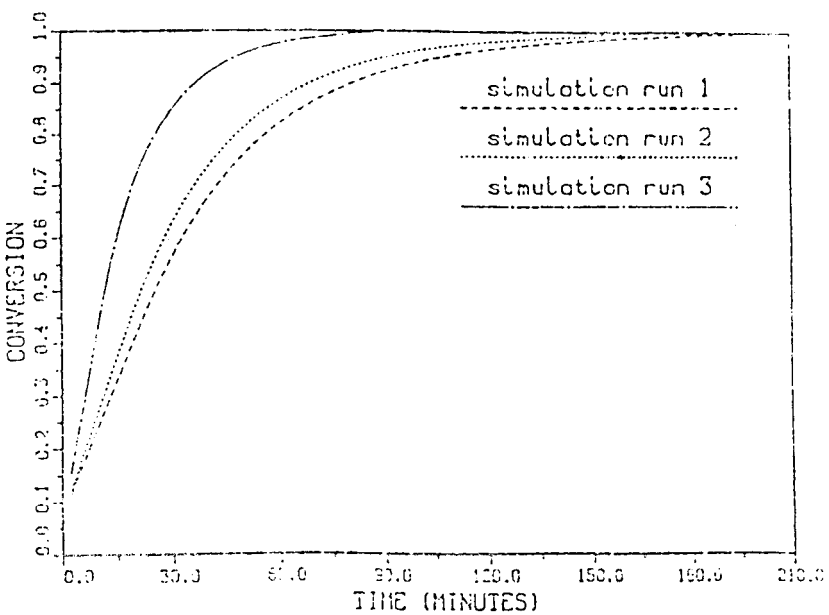

Figure 6 Conversion profiles for simulations 1, 2, and 3.

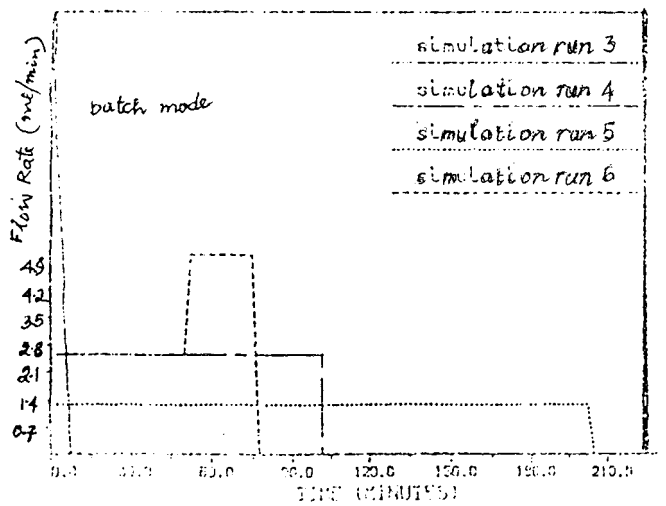

Figure 7 Feed rate profiles for simulations 3, 4, 5, and 6.

preserved with subsequent polymerization in preformed seeds, although the values of the range diminished significantly (from 13–15 to 1.7–3.1 nm).

Figures 5 and 6 show the volume-average diameter and the conversion profile for these runs. Both the volume-average diameter and the duration of reaction decrease from simulation 1 to simulation 3. This is mainly attributed to the greater number of seed particles in each subsequent run. The greater the number of particles, the greater the number of reaction sites, and thus the faster the rate and the lower the reaction time. Also, the greater the number of particles, the greater the number of sites among which the monomer gets distributed and thus the smaller the average diameter. The results of these simulations are summarized in Table III. These interesting results—that the shape of the distribution is preserved and the trends in the range are preserved but the final distribution is considerably narrower in the case of batch addition of monomer—became the motivation for considering the effects of monomer addition policies on PSD. Monomer is generally added in the semibatch mode in industrial reactors, and thus the study of the semibatch reactor mode where monomer is fed over a period of time is also industrially more relevant.

Effects of monomer addition policy on PSD

In this section, the effect of three different monomer addition policies are studied. The initial recipe and the initial particle size distribution are the same for all these three runs (simulation 3). The monomer feed rates are for "monomer-starved operation" of the reactor. The maximum rate for the batch case is 1.5 $\times$ 10^{-3} g mol^{-1} s^{-1} or about 10.5 mL/min (Fig. 8). Addition of monomer at a rate lower than this value will result in a monomer-starved operation. For simulations 4 and 5, the monomer addition rates are 2.5 and 1.25 mL/min, respectively. For simulation 6, half the monomer is fed at the rate of 2.5 mL/min initially and the remaining half is fed at the rate of 5.0 mL/min. It can be seen that the total reaction time increases with the decrease in monomer flow rate, as expected (Fig. 9). It can also be seen by comparing Figures 7 and 8, showing the feed rate profile and the reaction rate profile, respectively, that these two profiles match each other. This is the characteristic of monomer-starved addition policy. The monomer is added so slowly that as soon as it is added it reacts and none is left for accumulation to increase the monomer concentration in the growing particles during reaction or to form separate monomer droplets. With increased monomer addition rate, the rate of polymerization also increases as a result of the greater accumulation of monomer in the particles. Thus, by increasing the monomer addition rate, the polymerization time can be decreased, as has been shown here. This phenomenon, characterizing "monomer-starved addition policies," has been experimentally observed for styrene and methylmethacrylate.[15]

Figure 10 shows the PSD at the end of polymerization for the semibatch runs (simulations 4, 5, and 6). It appears from the figure that the PSDs are identical, but a closer look reveals the differences among the PSDs, which are given in Table III. Decreasing the monomer addition rate does not produce any perceptible change in the range of the distribution but the average size increases. This shows that the distribution becomes sharper or is narrower with slower monomer addition rate. Comparing these simulations with that for the batch case (simulation 3), this effect becomes more pronounced. The range in the batch

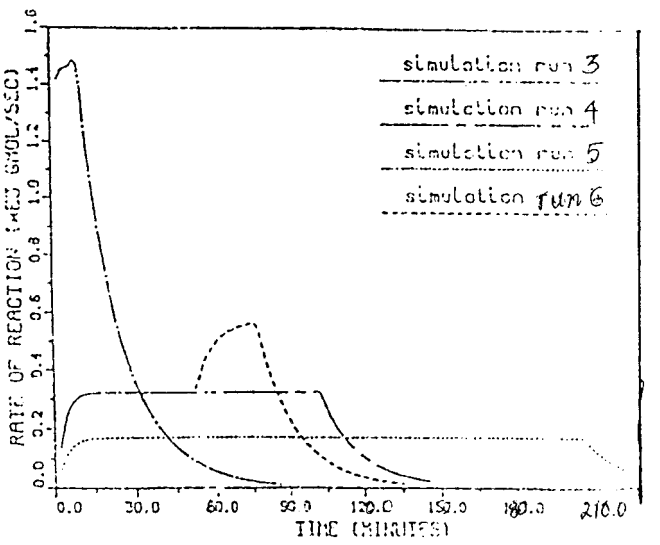

Figure 8 Reaction rate profiles for simulations 3, 4, 5, and 6.

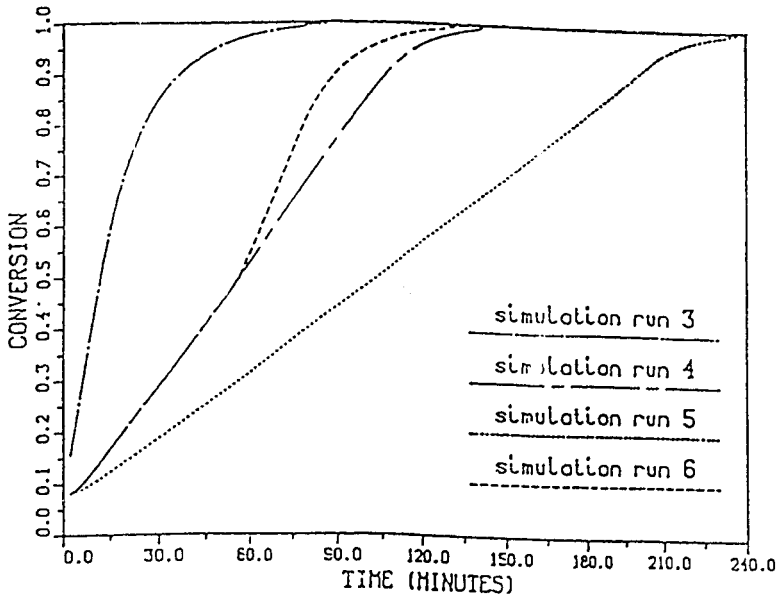

Figure 9 Conversion profiles for simulations 3, 4, 5, and 6.

case (infinite addition rate) is 3.1 nm, which is larger than the range for these runs (2.1 nm); therefore, by slowing the addition rate, it can be concluded that the distribution becomes narrower. An explanation of this effect can be provided as follows. With a decrease in the monomer addition rate, the duration of the growth stage increases, which makes the distribution narrower. These model-based effects have been reported earlier based on an experimental work[16] on the polymerization system styrene, PPS, and SLS (which is considered in this study) for bimodal seed particles. The present work involves particles that vary from micellar size to about 80 nm and is representative of a real reactor operation involving particles of various sizes, which are created *in situ*.

The conclusion of the previous authors was the same as that proposed in this work, that the final particle size distribution is narrowed down for the system considered. This work has shown this to be true for systems involving different initiator and emulsifier amounts and different monomer addition policies; the final PSD is always narrower than the initial PSD (obtained at the end of the nucleation period) for all cases. However, it has been further shown that the narrowing down of the final PSD can be controlled by varying the initiator amount, emulsifier amount, monomer addition mode, and monomer flow rate. The higher initiator amount, the lower emulsifier amount, the monomer addition in the semibatch mode, and the smaller monomer addition rate all give narrower final PSDs. The previous authors provided an explanation for the narrowing of the final PSD (i.e., the smaller particles grow at a faster rate than the larger particles), although, physically, this is not correct. The particle growth rate [given by eq. (15)] is a function of the average number of radicals in the particle (i), and the monomer volume fraction inside the particles (Φ): the smaller the particle size, the lower are the values of both these variables, and hence, the smaller is the growth rate of the smaller particles. The correct explanation, an outcome of this work, seems to be that the greater the length of the growth stage (lower monomer addition rates increase the length of the growth stage), compared to that of the nucleation stage (provided that the number of particles is the same; the nucleation period is the same for simulations 3, 4, 5, and 6), the narrower is the final PSD. The previous work used a seeded system to omit the intractable nucleation stage, whereas this work also incorporated the nucleation stage. Thus, the present work is more general and a closer representation of an actual reactor operation.

THE SELF-SHARPENING EFFECT

Let there be two particles, a and b, of volumes V_{a0} and V_{b0} ($V_{a0} < V_{b0}$) at a given time. After time t (from this time), their respective volumes are V_a and V_b. Consider the volumetric growth rate, $\mu \propto V^c$ or $\mu = kV^c$. Consider the variable V_b/V_a. Its derivative with time will determine whether it will decrease or increase with time. $d(V_b/V_a)/dt$ is given by $[V_a(dV_b/dt) - V_b(dV_a/dt)]/V_a^2$ or $(V_a\mu_b - V_b\mu a)/V_a^2$ or $(V_akV_b^c - V_bkV_a^c)/V_a^2$ or $kV_aV_b(V_b^{c-1} - V_a^{c-1})/V_a^2$. $0 \leq c < 1$ because, if $c = 1$, the volume will grow exponentially, and if $c > 1$, it will grow at an even faster rate, which has no physical meaning, and when $c < 0$, smaller particles will grow at a faster rate than the larger particles,

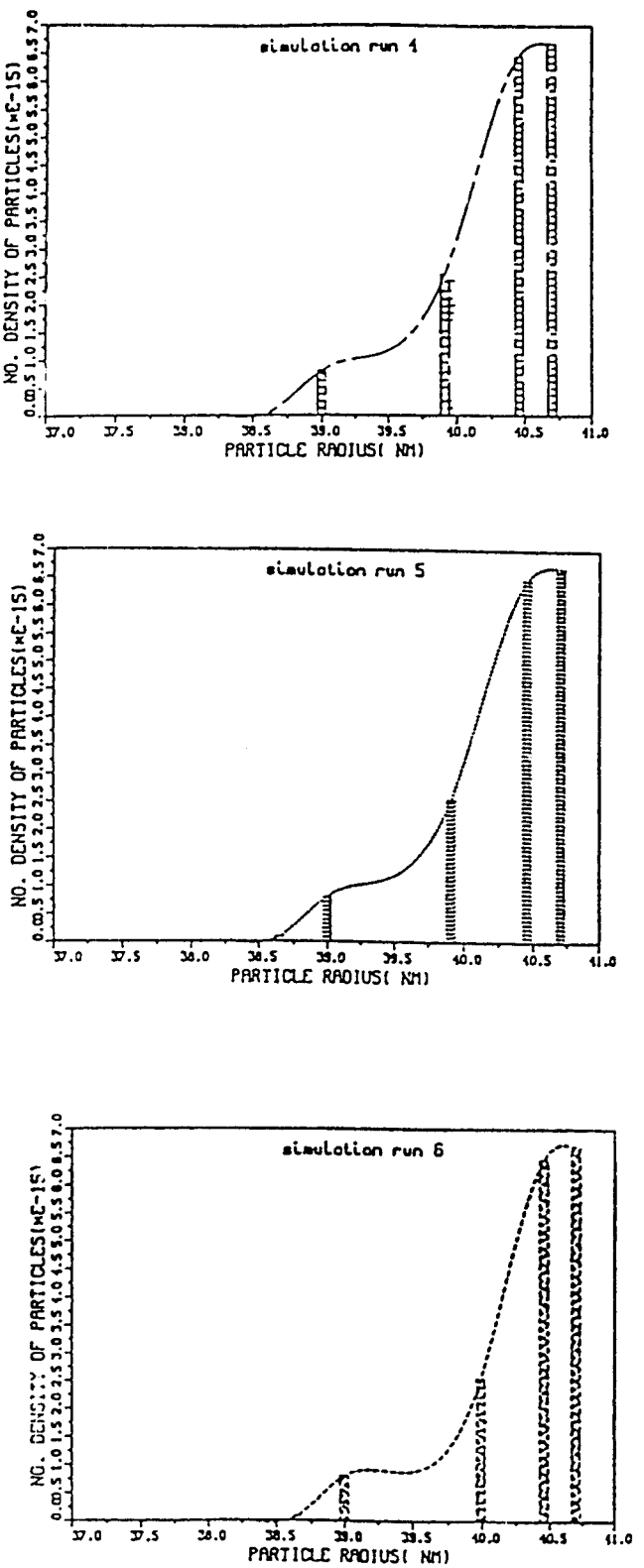

Figure 10 Full particle size distribution (final) for simulations 4, 5, and 6.

which again has no physical meaning. V_b/V_a will decrease with time because $c - 1$ is a negative number, which implies that the derivative is negative; that is, $V_b^{c-1} - V_a^{c-1} < 0$, or $(V_b/V_a)^{c-1} < 1$, which is correct because any positive number ($V_b > V_a$) raised to a negative power is less than 1. The variable V_b/V_a was used here as a measure of the spread of the distribution.

Previous investigators used the variable D_b/D_a and found experimentally that it decreased with time.[16] Directly, in terms of D_b/D_a, we can see that $d(D_b/D_a)/dt = [(D_a dD_b/dt) - (D_b dD_a/dt)]/D_a^2$. $\mu = dV/dt = d(\pi/6D^3)/dt = \pi/2D^2(dD/dt) = kV^c = k(\pi/6D^3)^c$. Thus, $dD/dt = k'D^{c'}$, where $k' = 3k(\pi/6)^{c-1}$ and $c' = 3c - 2$. Given that $0 \le c < 1$, $c' > 0$, when $\frac{2}{3} < c < 1$ and $c' \le 0$ when $0 \le c \le \frac{2}{3}$. Therefore, $d(D_b/D_a)/dt = [(D_a dD_b/dt) - (D_b dD_a/dt)]/D_a^2 = [(D_a k' D_b^{c'}) - (D_b k' D_a^{c'})]/D_a^2 = k' D_a D_b (D_b^{c'-1} - D_a^{c'-1})/D_a^2$. Now, $c' - 1 = 3(c - 1)$, which is always less than 0 because $c < 0$. Therefore, $d(D_b/D_a)/dt < 0$ or D_b/D_a will always decrease with time, as found by previous workers.[16] They interpreted their results by saying that the growth rate favors smaller particles over larger particles or smaller particles grow at a faster rate than the larger particles, which is not physically correct. In a recent work,[20] the effect of monomer feed rate on the parameter D_b/D_a has been studied and it was found to decrease with time, although this was again explained based on the previous explanation.[16] The correct nature of the growth and correct mathematical interpretation is provided above.

In this work, the range [maximum diameter (D_L) − minimum diameter (D_S)]/2 is used as the measure of the spread of the distribution. Let us use $V_L - V_S$. [Note: $D_L - D_S = 6/\pi(V_L - V_S)/(D_L^2 + D_L D_S + D_S^2)$.] Whether $V_L - V_S$ (or $D_L - D_S$) will decrease with time or increase with time will depend on the sign of its time derivative. $d(V_L - V_S)/dt = \mu_L - \mu_S$, which is positive (growth rate of larger particles is, in general, greater than that of the smaller particles); therefore $V_L - V_S$ is an increasing function of time. $d(D_L - D_S)/dt = (dD_L/dt) - (dD_S/dt)$. $\mu = dV/dt = d(\pi/6D^3)/dt = \pi/2D^2(dD/dt) = kV^c = k(\pi/6D^3)^c$. Thus, $dD/dt = k'D^{c'}$, where $k' = 3k(\pi/6)^{c-1}$ and $c' = 3c - 2$. Given that $0 \le c < 1$, $c' > 0$, when $\frac{2}{3} < c < 1$ and $c' \le 0$ when $0 \le c \le \frac{2}{3}$. Thus, $d(D_L - D_S)/dt = k'D_L^{c'} - k'D_S^{c'} > 0$ when $c' > 0$ or when $\frac{2}{3} < c < 1$, for which $D_L - D_S$ will increase with time; otherwise, it will decrease with time. In the simulations, the dependency of monomer concentration with size was neglected and when the exit rate constant is 0, the average number of radicals per particle is 0.5. Therefore, the growth rate for all the particles is identical: $V_L = V_{L0} + \mu t$, $V_S = V_{S0} + \mu t$, and $V_L - V_S = V_{L0} - V_{S0}$ = constant. Because $D_L - D_S = 6/\pi[(V_L - V_S)/(D_L^2 + D_L D_S + D_S^2)]$, which for our case reduces to $6/\pi[(\text{constant})/(D_L^2 + D_L D_S + D_S^2)]$. As D_L and D_S increase with time, the range $D_L - D_S$ decreases with time. Directly in terms of $D_L - D_S$, here $c = 0$ ($< \frac{2}{3}$) and $c' = -2 < 0$, and thus it will decrease with time. This explains why the range of the final

PSD for the simulations is always lower than that of the initial PSD.

In this section, it is shown that spread in the distribution, when expressed as V_a/V_b and D_a/D_b, will always decrease with time, whereas when expressed as $V_L - V_S$ it will increase with time (and when growth rate is size independent, it will remain constant). When expressed as $D_L - D_S$ the distribution will increase or decrease depending on the value of c. Thus, this self-sharpening effect is dependent on the variables used to express the spread. A number of variables are used in emulsion polymerization literature to express the spread of the distribution; four of these have been given above, whereas others are standard deviation, coefficient of variation, and polydispersity index.

It is well known that with the increase in initiator amount or decrease in the emulsifier amount, the PSD becomes narrower and this is explained qualitatively in terms of the decrease in the nucleation period. For the same nucleation period, however, the PSD is narrower for the semibatch addition compared to that in the batch addition and is narrower for lower monomer addition rate. Thus, a lower monomer addition rate gives a narrower PSD, which is a new result. This has been explained qualitatively in terms of increase in the growth period (or decrease in the growth rate) with slower addition of monomer because that is the only evident difference. Now, a quantitative proof is provided for this result. We wish to find how $V_L - V_S$ varies with the growth rate. Because $\mu = kV^c$, $V = (1/k)^{1/c}\mu^{1/c}$ and $dV/d\mu = (1/k)^{1/c}(1/c)\mu^{1/c-1} = (1/c)V/\mu = 1/(kcV^{c-1})$ and $d(V_L - V_S)/d\mu = 1/kc[(1/V_L^{c-1}) - (1/V_S^{c-1})]$, which is always greater than 0. Thus, $V_L - V_S$ will increase with increase in growth rate (or with increase in monomer addition rate) and will be maximum for the batch addition mode. For our case, it is more important to see how $D_L - D_S$ will vary with the growth rate. $\mu = kV^c = k'D^{3c}$ and $D = (\mu/k')^{1/3c}$. $dD/d\mu = \frac{1}{3}c(1/k')^{1/3c}\mu^{1/3(\text{cminus}1)} = \frac{1}{3}(cD/\mu)$. Therefore, $d(D_L - D_S)/d\mu = \frac{1}{3}c[(D_L/\mu_L) - (D_S/\mu_S)]$, which is positive if $D_L/\mu_L > D_S/\mu_S$ or $D_L/D_S > \mu_L/\mu_S = (D_L/D_S)^{3c}$ or if $1 > 3c$ or $c < \frac{1}{3}$. In our case the growth rate, as explained earlier, is independent of size, and thus $c = 0$ ($<\frac{1}{3}$). Thus, $D_L - D_S$ will increase with growth rate (or monomer flow rate) and will be maximum for the batch mode, which was also deduced from the simulations. Thus, this new result was also explained mathematically.

EXPERIMENTAL ANALYSIS OF PARTICLE SIZE DISTRIBUTIONS

The growth of previously prepared, 92-nm polystyrene latex (Dow LS-1030-B) was monitored[21] using the capillary hydrodynamic flow fractionation (CHDF) technique. This standard was cleaned using a serum-replacement cell, which ensures the removal of surface active agents absorbed onto the surface of the particles. The conductivity of the latex was measured to be 34 μS. The seeded polymerization was performed in the semibatch mode at 50°C. The recipe and the styrene monomer feed rates were designed to ensure monomer-starved conditions throughout the course of reaction because interference attributed to the presence of an excess of monomer can lead to noisy, error-prone measurements. This was done by maintaining the monomer feed rate lower than the maximum rate of polymerization. To keep complications like coagulation and reactor fouling from masking these initial attempts at monitoring, the polymerizations were carried out at low solids content. Unimodal particle growth was ensured by providing sufficient emulsifier so as to prevent coagulation while maintaining free emulsifier concentration. The monitoring scheme involved sampling at intervals during the course of the reaction followed immediately by particle size analysis. Table IV shows the recipe used.

TABLE IV
Recipe Used for Semibatch Polymerization

Ingredient	Amount (g)
Dow latex (92 nm) (seed: LSD-1039-B)	20
Styrene (feed)	24.01
Emulsifier: sodium dodecyl sulfate	1.00
Initiator: $K_2S_2O_8$	1.0061
Buffer: $NaHCO_3$	1.0005
DDI water	480.00

Figure 11 shows the profile of some of the key variables during the semibatch process. The plots are experimental values obtained using gravimetric analysis. Figure 11(a) shows three variables: (1) a dashed line showing the cumulative increase of the monomer (fed at a constant rate of 0.16 g/min for a total feed time of 145 min); (2) a dotted line showing the instantaneous amount of polymer formed; and (3) a solid line showing the difference between (1) and (2) that translates into the amount of residual monomer at any instant of time. Figure 11(b) plots the development of polymer during the reaction. Three distinct regimes are evident from the solids profile: (1) regime 1, with a minimal slope, extending up to 45 min of the reaction time; (2) regime 2 showing the maximum slope from 45 to 145 min, corresponding to the maximum rate of polymerization corresponding to the feed rate; and (3) regime 3, which takes effect when the monomer feed is exhausted to the completion of the reaction (145–210 min).

Figure 12 plots the particle size distribution (by weight) obtained using the CHDF. Consider the first stage of reaction, regime 1. As indicated earlier, this stage corresponds to the lowest rate of reaction constituting the first 50 min, approximately. Figure 12

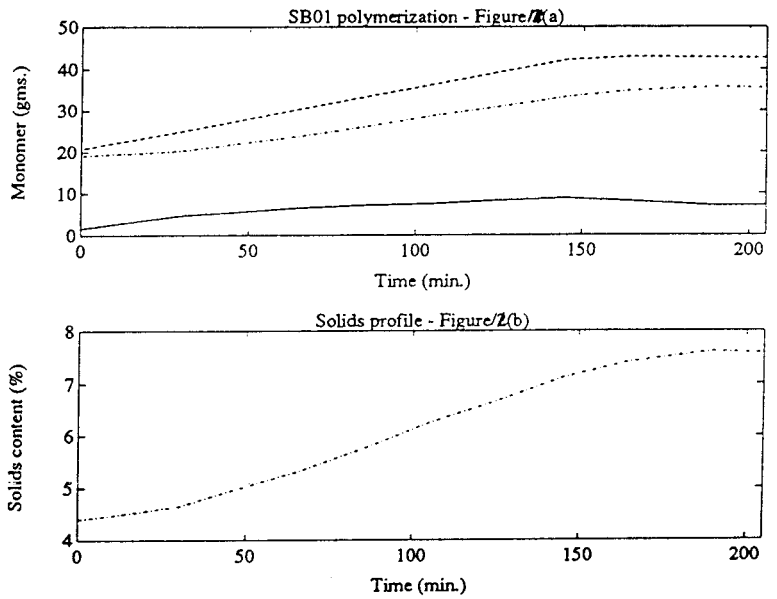

Figure 11 (a) Profiles of the monomer feed rate (dashed), polymer formation rate (dotted), and residual monomer amount (solid). (b) Profile of the development of solids content during the course of the reaction.

shows the particle size distributions corresponding to the seed (solid line) and those for samples taken after 25 min (dashed) and 50 min (dotted). The graphs show a gradual progression toward larger diameters. During this interval, the particles primarily undergo swelling by monomer. Next, regime 2 (45–145 min) is considered. Fractograms belonging to this regime are shown in Figure 13. Sampling times of 90 min (solid), 110 min (dashed), and 130 min (dotted) are shown to represent this regime of interest. During this period the monomer-swollen particles are polymerized. Regime 3, the final stage of polymerization (after 145 min), is characterized in Figure 14, which plots the distributions corresponding to 150 min (solid), 170 min (dashed), and 195 min (dotted). The monomer being fed to sustain growth is exhausted after 145 min and therefore in this final stage of the reaction the residual monomer in the system is converted to polymer. The overall characterization of the reaction with respect to the particle size distribution is depicted in

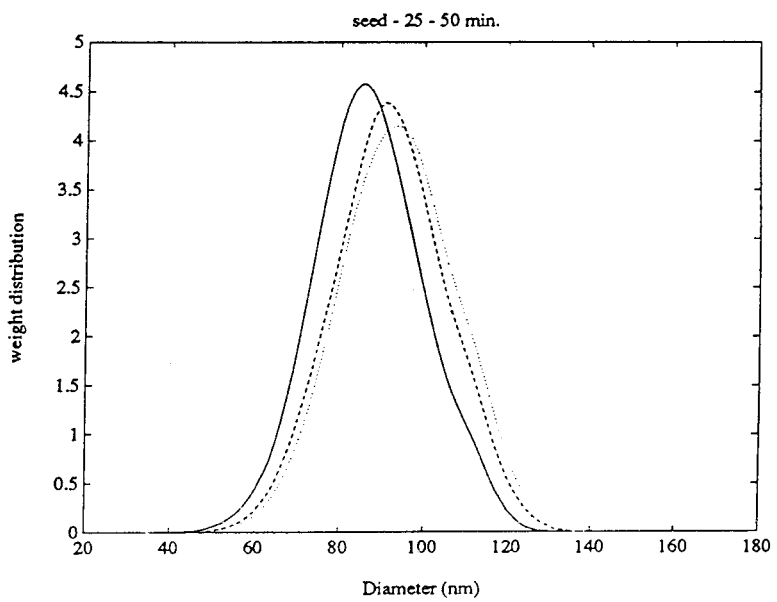

Figure 12 Growth of particle size distribution monitored in the first regime: seed (solid), 25 min (dashed), and 50 min (dotted).

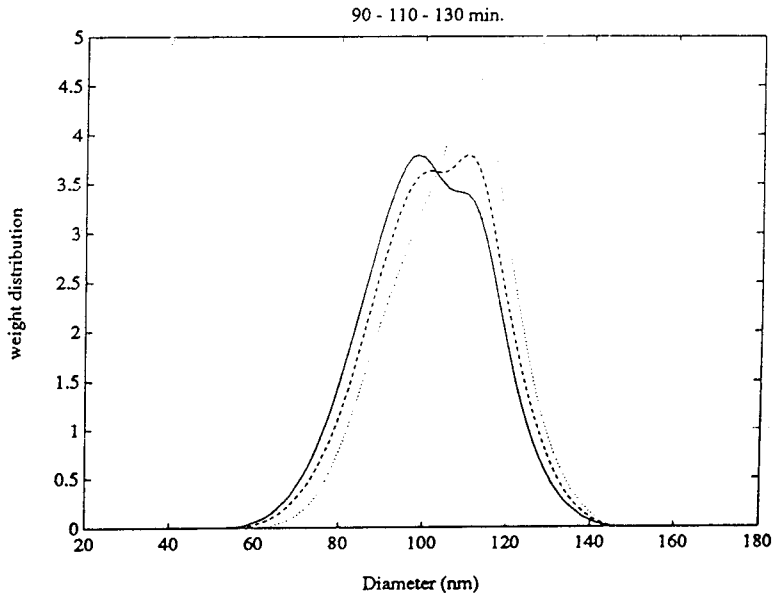

Figure 13 Growth of particle size distribution monitored in the second regime: 90 min (solid), 110 min (dashed), and 130 min (dotted).

Figure 15. The four distributions are representative of the various regimes of the reaction. The number-average diameters (×) and weight-average diameters (○) are plotted as a function of reaction time in Figure 16. The curve displays the expected monotonic increase in particle diameter. Two interesting features to be noted in this graph are the existence of two local maxima at the two extremes, one occurring between 0 and 50 min and the other occurring between 150 and 210 min.

These are not experimental artifacts, and can be explained because of the shrinkage effect. This effect occurs between the monomer–polymer systems, where the density difference between monomer and its polymer is significant, which is true of styrene. Because of this density difference, the volumetric size of the monomer droplet is larger than its corresponding polymer particle. Accordingly, monomer-swollen polymer particles will occupy a larger volume than that of the fully converted polymer particles. The presence of a local maximum in the data plotted in Figure 16, during the initial stages of the reaction, reconfirms the presence of monomer-swollen particles in this pe-

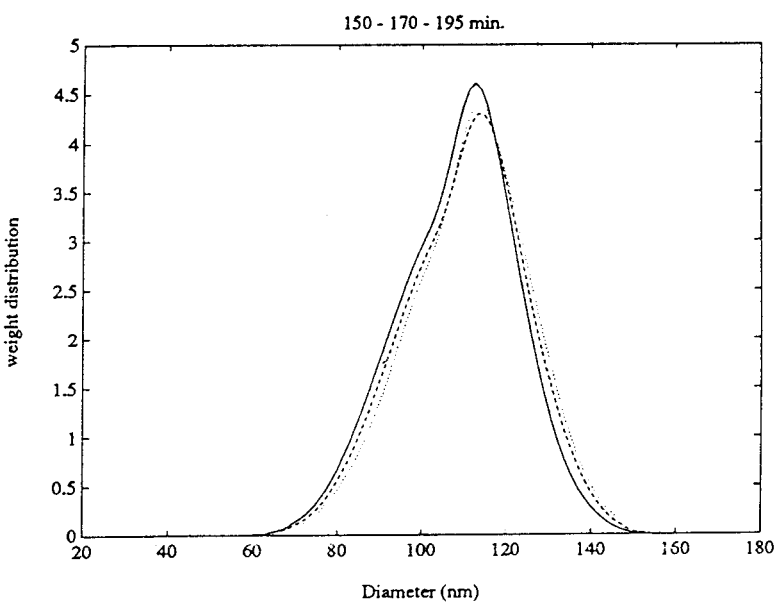

Figure 14 Growth of particle size distribution monitored in the third regime: 150 min (solid), 170 min (dashed), and 195 min (dotted).

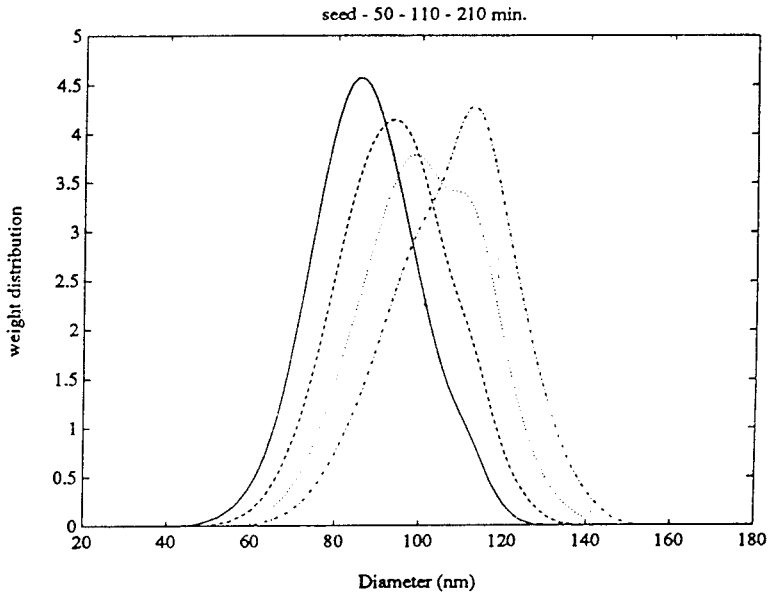

Figure 15 Particle size distributions at representative times during the course of polymerization: seed (solid), 50 min (dashed), 110 min (dotted), and 210 min (dotted-dashed).

riod. The other maximum occurs around 190 min, at which point the particles are now swollen with the remainder of the monomer after the continuous feed was stopped at 145 min. Figure 17 shows the polydispersity index as a function of reaction time. Values closer to 1 imply more monodisperse distributions. The figure shows values around 1.05 through most of the reaction. This demonstrates that the growth pattern monitored was indeed unimodal without generation of new particles.

In this work, it has been shown that the variable $D_L - D_S$ decreases during the course of the run. In Table V, the values of D_S, D_L, and $D_L - D_S$ at various times corresponding to these distributions are given. It can be seen that after the initial swelling phase, the variable $D_L - D_S$ decreases throughout the run and the final value of the range is lower than the initial value. This provides experimental evidence in support of the model-based conclusions. The average volumetric growth rate for the smallest size particle was 667 nm^3/min and that for the largest particle was 3700 nm^3/min.

The practical significance of this work is as follows. This work can serve as a guide for both researchers

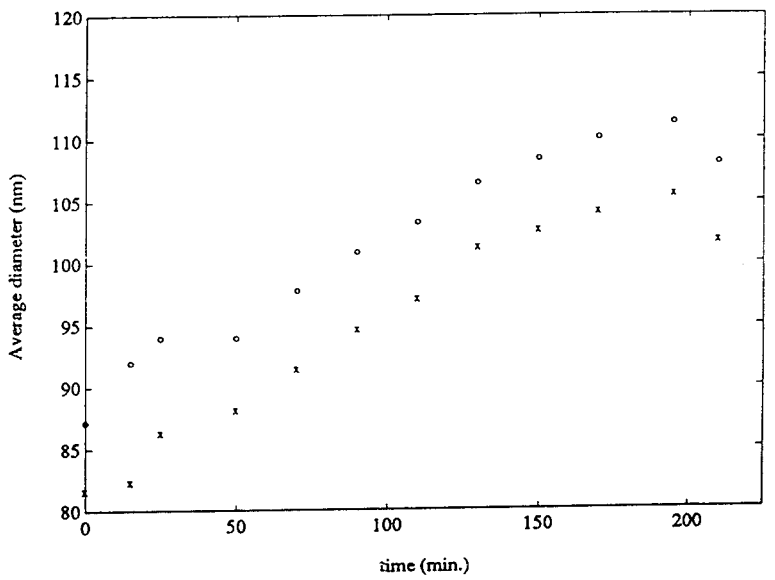

Figure 16 Illustration showing the particle growth patterns in terms of the weight-average diameter (○) and the number-average diameter (×).

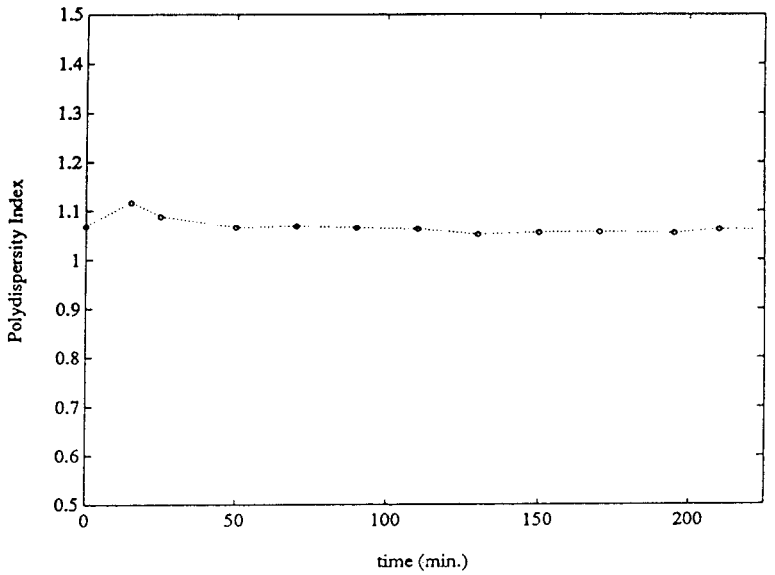

Figure 17 Plot of polydispersity index as a function of reaction time.

and industrial practitioners in designing reactor charging and operating policies with regard to the initiator charge, emulsifier charge, and monomer addition modes and rates that would give a narrower or a broader PSD. The higher initiator amount, the lower emulsifier amount, the monomer addition in the semibatch mode, and the lower monomer addition rates all give narrower final PSDs. Narrow or monodisperse latices are used as size-calibration standards, and also find extensive use as model colloids to test theories in colloids and rheological studies. Broad latices are used to obtain high solid loading. It has been shown conclusively why and when PSD will narrow down during the run and why and when it will narrow down with the decrease in monomer flow rate. Attention must be given to the variable used for characterizing the PSD. Very little attention has been paid to PSD because both theoreticians and experimentalists prefer monodisperse systems. It is hoped that this work will stimulate greater interest among researchers and industrial practitioners for considering full PSD, given that real systems are polydisperse in general.

TABLE V
Variation of D_S, D_L, and $D_L - D_S$ with Time for Experimental Distributions

Time (min)	D_S (nm)	D_L (nm)	$D_L - D_S$ (nm)
Seed	43.08	127.09	84.01
25	47.69	133.85	86.16
50	50.77	138.46	87.09
90	53.85	143.07	89.22
110	58.46	144.15	85.59
130	63.05	146.15	83.10
150	63.50	146.15	82.65
170	64.02	146.15	82.13
190	66.15	147.69	81.54

CONCLUSIONS

A mathematical model that accounts for the development of particle size distribution in batch and semibatch emulsion polymerization reactor was developed. The model includes such mechanistic details as generation of particles from radicals entering micelles; particle-size dependency of the radical entry mechanisms; coupling of the radical concentrations in the aqueous and the particle phases; determination of the particle phase radical concentration by radical entry into, exit from, and termination inside the particles; and thermodynamic equilibrium between the monomer concentration in the aqueous phase and the particle phase. The model was solved using orthogonal collocation and was used to study the effects of several operating variables on the initial and the final particle size distributions. Full PSDs were reported that were normally omitted in earlier studies. It was shown through simulations that the initial initiator amount and the emulsifier amount can control the broadness of the distributions (both initial and final PSDs). The higher initiator amounts and the lower emulsifier amounts favor narrower distributions. The model-based conclusions regarding monomer addition policies are that addition of monomer in the semibatch mode, compared to the batch mode, and further, lower monomer addition rates, favor narrower distributions (lower ranges) and larger average-size particles, which together constitute a new result.

It was further shown through simulations that under monomer-starved conditions the reaction rate

closely matched the monomer feed rate. The final PSDs were always considerably narrower than the initial PSDs. The shape of the distribution was preserved. These conclusions may be explained as follows: (1) qualitatively—the shorter the length of the nucleation stage and the larger the length of the growth stage (provided the number of particles remains the same), the narrower the PSD; and (2) mathematically—in terms of the "self-sharpening" effect, which depends on the variable used to express the spread in the distribution. The time derivatives of these variables were found to be negative for the case considered, which proved that the PSD narrows down with time, and further the derivatives of these variables, with respect to growth rate, were found to be positive for the case considered, which proved that the PSD narrows down with increased flow rate and a batch operation will give a narrower PSD than will a semibatch operation. This is true if we use V_b/V_a, D_b/D_a, or $V_L - V_S$ as the measure of the spread of the distribution. If we use $D_L - D_S$ as the size variable, then this is true only when the variable c in the relation $dV/dt = kV^c$ is less than $\frac{1}{3}$ or else the PSD when measured in terms of $D_L - D_S$ will broaden with decrease in flow rate. This is a new result and, further, the correct explanation of the self-sharpening effect is provided for the first time. Experimental particle size distributions were analyzed in detail and evidence in support of the self-sharpening effect was provided.

NOMENCLATURE

a_{em}	emulsifier coverage area on a micelle, cm^2 $molecule^{-1}$
a_{ep}	emulsifier coverage on a particle, cm^2 $molecule^{-1}$
A_m	total surface area of micelles, cm^2
A_p	total particle surface area, cm^2
E_{cmc}	critical micelle concentration, g cm^2
c	volume dependency power of volumetric growth rate
D	particle diameter, nm
f	initiator decomposition efficiency
$F(v, t)V_R\, dv$	number of particles with size between v and $v + dv$
$F(t', t)V_R\, dt'$	number of particles with birth time between t' and $t' + dt'$
i	average number of radicals per particle
$[I]$	initiator concentration in the reactor, g mol^{-1} cm^{-3}
k	proportionality constant of volumetric growth rate
k_d	initiator decomposition rate constant, s^{-1}
k_{de}	exit rate coefficient, s^{-1}
k_e	entry rate coefficient, s^{-1}
k_{mm}	mass transfer coefficient for radical capture by micelles, cm^2 s^{-1}
k_{mp}	mass transfer coefficient for radical capture by particles, cm^2 s^{-1}
k_p	propagation rate constant, cm^3 g^{-1} mol^{-1} s^{-1}
k_t	termination rate constant in the particle, cm^3 g^{-1} mol^{-1} s^{-1}
k_{tw}	termination rate constant in the aqueous phase, cm^3 g^{-1} mol^{-1} s^{-1}
m_p	mass of polymer in particles, g
$[m]$	micelle concentration in the reactor, g mol^{-1} cm^{-3}
$[M]_D$	monomer concentration in the droplet phase, g mol^{-1} cm^{-3}
$[M]_P$	monomer concentration in the particle phase, g mol^{-1} cm^{-3}
$[M]_R$	monomer concentration in the reactor, g mol^{-1} cm^{-3}
$[M]_W$	aqueous phase monomer concentration, g mol^{-1} cm^{-3}
$[M]_{\text{sat}}$	aqueous phase monomer concentration at saturation, g mol^{-1} cm^{-3}
n	exponent determining whether radical capture is diffusion controlled or collision controlled
N_a	Avogadro's number molecule, g mol^{-1}
Q_E	volumetric flow rate of emulsifier, cm^3 s^{-1}
Q_I	volumetric flow rate of initiator, cm^3 s^{-1}
Q_M	volumetric flow rate of monomer, cm^3 s^{-1}
r	particle radius, cm
r_m	micelle radius, cm
$[R]$	aqueous phase radical concentration, g mol^{-1} cm^3
R_{em}	rate of radical capture by micelles, s^{-1}
R_{ep}	rate of radical capture by particles, s^{-1}
R_n	rate of micellar nucleation, g mol^{-1} s^{-1}
R_p	rate of polymerization, g mol^{-1} s^{-1}
R_g	rate of particle mass growth, g s^{-1}
R_G	gas constant, cal g^{-1} mol^{-1}
t	time, s
t'	birth time, s
v, V	particle volume, cm^3
v'	particle volume, cm^3
V_D	volume of monomer droplets, cm^3
V_P	polymer volume, cm^3
V_R	reactor volume, cm^3
V_W	aqueous phase volume, cm^3

Greek letters

γ	interfacial tension, dyn cm^{-1}
ρ	monomer density, g cm^{-3}
ρ_p	polymer density, g cm^{-3}
μ	volumetric growth rate

χ	Flory–Huggins constant
Φ	monomer volume fraction in the particle

Subscripts

cmc	critical micelle concentration
E	emulsifier
I	initiator
M	monomer
P	particle
R	reaction medium
W	aqueous phase
L	large particle
S	small particle

References

1. Sood, A. In: Model of Viscosity of Bimodal Dispersion for Improved Flow Behaviour, National Symposium on Polymer Science, Sardar Patel University, Vallabh Vidyanagar, Gujarat, India, December 3–4, 2002.
2. Sood, A. In: Low Viscosity Giving Efficient Operating Procedure for Highly Viscous Emulsion Polymerization, National Symposium on Polymer Science, Sardar Patel University, Vallabh Vidyanagar, Gujarat, India, December 3–4, 2002.
3. Sood, A. In: Stability of the Miniemulsion Droplet Size Distribution, Proceedings/Abstracts of CHEMCON-2001, Indian Institute of Chemical Engineers, Chennai, India, December 19–22, 2001.
4. Sood, A. Indian Chem Eng 2002, 44, 75.
5. Sood, A. In: Modeling Particle Nucleation in Emulsion Polymerization: An Approach Based on Comprehensive Nucleation Theory, POLYCON-2002, National Symposium on Recent Developments of Polymers, Harcourt Butler Technological Institute, Kanpur, India, August 16–17, 2002.
6. Brooks, B. W. Br Polym J 1970, 2, 197.
7. Brooks, B. W. Br Polym J 1971, 3, 269.
8. Min, K. W.; Ray, W. H. J Macromol Sci Rev Macromol Chem 1978, 22, 89.
9. Morton, M.; Kaizerman, S.; Altier, M. W. J Colloid Sci 1954, 9, 300.
10. Smith, W. V.; Ewart, R. H. J Chem Phys 1948, 16, 592.
11. Stockmayer, W. H. J Polym Sci 1957, 24, 314.
12. O'Toole, J. T. J Appl Polym Sci 1965, 9, 1291.
13. Ugelstad, J.; Mork, P. C.; Aasen, J. O. J Polym Sci Part A-1 1967, 5, 2281.
14. Rawlings, J. B.; Ray, W. H. Polym Eng Sci 1988, 28, 237.
15. Gerrens, J. L. J Polym Sci Part C 1969, 27, 77.
16. Vanderhoff, J. W.; Vitkuske, J. F.; Bradford, E. B.; Alfrey, T., Jr. J Polym Sci 1956, XX, 225.
17. Prindle, J. C. Ph.D. Dissertation, University of Wisconsin, Madison, 1989.
18. Paquet, D. A., Jr.; Ray, W. H. AIChE J 1994, 40, 88.
19. Saldivar, E.; Ray, W. H. Ind Eng Chem Res 1997, 36, 1322.
20. Liotta, V. Ph.D. Dissertation, Lehigh University, Bethlehem, PA, 1996.
21. Venkatesan, J.; Sood, A.; Silebi, C. A.; El-Aasser, M. S.; Georgakis, C. In: Proceedings of the AIChE Annual Meeting, Los Angeles, CA, 1990.